molecular pharmaceutics

Brief Article

pubs.acs.org/molecularpharmaceutics

In Vivo Pulmonary Delivery and Magnetic-Targeting of Dry Powder Nano-in-Microparticles

Dominique N. Price,[†] Loreen R. Stromberg,[†,‡] Nitesh K. Kunda,[†] and Pavan Muttil*[,†,§]

[†]Department of Pharmaceutical Sciences, College of Pharmacy, University of New Mexico Health Sciences Center, Albuquerque, New Mexico 87131, United States

[‡]Department of Mechanical Engineering, Iowa State University, Ames, Iowa 50011, United States

[§]The University of New Mexico Comprehensive Cancer Center, Albuquerque, New Mexico 87131, United States

Supporting Information

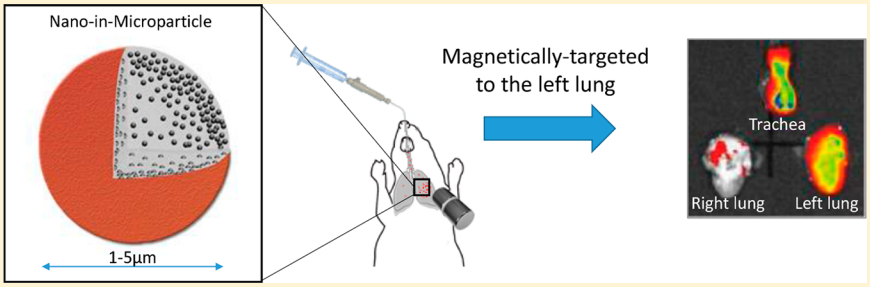

ABSTRACT: This brief communication evaluates the cytotoxicity and targeting capability of a dry powder chemotherapeutic. Nano-in-microparticles (NIMs) are a dry powder drug delivery vehicle containing superparamagnetic iron oxide nanoparticles (SPIONs) and either doxorubicin (w/w solids) or fluorescent nanospheres (w/v during formulation; as a drug surrogate) in a lactose matrix. *In vitro* cytotoxicity was evaluated in A549 adenocarcinoma cells using MTS and LDH assays to assess viability and toxicity after 48 h of NIMs exposure. *In vivo* magnetic-field-dependent targeting of inhaled NIMs was evaluated in a healthy mouse model. Mice were endotracheally administered fluorescently labeled NIMs either as a dry powder or a liquid aerosol in the presence of an external magnet placed over the left lung. Quantification of fluorescence and iron showed a significant increase in both fluorescence intensity and iron content to the left magnetized lung. In comparison, we observed decreased targeting of fluorescent nanospheres to the left lung from an aerosolized liquid suspension, due to the dissociation of SPIONs and nanoparticles during pulmonary administration. We conclude that dry powder NIMs maintain the therapeutic cytotoxicity of doxorubicin and can be better targeted to specific regions of the lung in the presence of a magnetic field, compared to a liquid suspension.

KEYWORDS: *targeted pulmonary delivery, nano-in-microparticles (NIMs), pulmonary chemotherapeutic, aerosolized drug delivery, non-small cell lung cancer, superparamagnetic iron oxide nanoparticles (SPIONs)*

INTRODUCTION

Lung cancer is the second most commonly diagnosed cancer in both men and women, and it has the highest mortality rate compared to all other types of cancer accounting for 26.5% of all cancer deaths.[1−3] Conventional chemotherapy for lung cancer is administered intravenously and does not distinguish between cancerous and healthy cells. The high concentrations of chemotherapeutic agents that are required for systemic administration often lead to non-specific adverse effects, while lung tumor microenvironments that are distantly located from capillaries receive subtherapeutic drug concentrations.

Pulmonary drug delivery has been used to treat respiratory diseases, such as asthma and microbial infections, as well as systemic diseases.[4−9] The lungs are well-suited for drug delivery due to their large surface area, thin alveolar epithelium, easily permeable membrane, and extensive vasculature, which allow substantial and rapid drug absorption for increased local and systemic efficacy.[9] Pulmonary delivery of chemotherapy has been evaluated in human trials for the treatment of lung cancer.[10−15] A phase I/II study of inhaled doxorubicin combined with systemic platinum-based therapy was administered to twenty-eight patients with advanced non-small cell lung cancer.[11] However, while the results of this localized delivery were promising, a few patients experienced dose-limiting pulmonary-toxicity. In a preclinical study, Dames and colleagues attempted to minimize toxicity to the whole lung by targeting a therapeutic surrogate to a specific lung lobe in mice using iron oxide nanoparticles in the presence of an external magnetic field.[16] However, targeting to the magnetized lobe

Received: June 23, 2017
Revised: October 23, 2017
Accepted: October 25, 2017
Published: October 25, 2017

DOI: 10.1021/acs.molpharmaceut.7b00532
Mol. Pharmaceutics 2017, 14, 4741−4750

was minimal due to the separation of the drug surrogate and iron oxide nanoparticles during pulmonary administration of the liquid suspension.

The aim of this study was 2-fold, (1) to determine if dry powder nano-in-microparticles (NIMs)[17] containing doxorubicin still display therapeutic cytotoxicity after the spray drying process, and (2) to evaluate the magnetic-field-dependent targeting of dry powder NIMs administered endotracheally into the lungs of healthy mice (Figure 1A). Our hypothesis was that

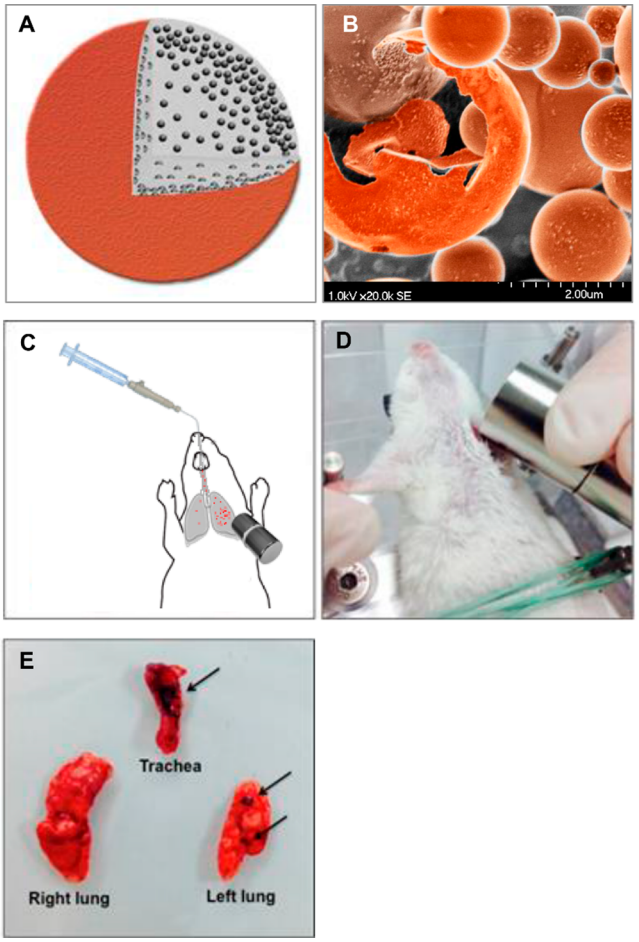

Figure 1. Magnetic field-dependent lung targeting. (A) Pictorial representation of NIMs dry powder showing lactose (gray), doxorubicin (red), and SPIONs (black).[17] (B) Scanning electron microscope image of NIMs dry powder. (C) Schematic of endotracheal delivery of magnetically-targeted NIMs. (D) Orientation of the permanent magnet in thoracotomized mice prior to pulmonary delivery of NIMs. (E) Orientation of the trachea, right lung, and left lung prior to imaging. SPIONs are visible in the trachea and left lung (shown by arrows) demonstrating magnetic targeting.

the incorporation of a chemotherapeutic agent and iron-oxide nanoparticles in a powder matrix should prevent the separation of nanoparticles and therapeutic observed by Dames et al., while still targeting the drug payload to the magnetized lung region (Figure 1A).[16] This inhalable drug delivery approach has the potential to reduce toxicity to healthy tissues by targeting drugs directly to specific regions of the lung, thus achieving therapeutic concentrations near solid tumors (Figure 1B).[18,19]

EXPERIMENTAL METHODS

Materials. Alpha-D-(+)-lactose monohydrate Respitose ML-001 was a gift from DMV-Fonterra Excipients GmbH & Co. KG (Goch, Germany). FluidMAG-UC SPIONs with a hydrodynamic diameter of 50 nm was purchased from Chemicell GmbH (Berlin, Germany). Fluorescent dye-containing NIMs were formulated with Molecular Probes FluoSpheres Carboxylate-Modified Nanospheres (F8783, 0.02 μm, λ_{ex} = 660 nm and λ_{em} = 680 nm, Molecular Probes, Life Technologies, Thermo Fisher Scientific, Inc. Waltham, MA, USA).

Formulation and Characterization of the NIMs Delivery Vehicle. Spray drying of the NIMs delivery vehicle was performed as described previously.[17] Briefly, a suspension containing approximately 20% (w/w) SPIONs and either 2.8% (w/w) doxorubicin (Selleck Chemicals, LLC, Houston, TX, USA) (for *in vitro* studies) or 10% (w/w) fluorescent nanospheres (fluorescent drug surrogate for *in vivo* studies) was spray-dried in Milli-Q water and a lactose matrix (2.5% w/v total feed concentration) (Figure 1A). A B-290 mini-spray dryer with a standard two-fluid nozzle (0.7 mm diameter) (Büchi Corporation, Flawil, Switzerland) was used to spray dry the suspension with the following parameters: inlet temperature 170 ± 2 °C, outlet temperature 103 ± 2 °C, aspirator rate 100%, and an atomization air flow rate of 742NL/h. Spray-dried control microparticles were formulated containing a higher concentration of 5% lactose only (w/v) in Milli-Q water to keep particle sizing similar.

Dry Powder NIMs Particle Sizing. NIMs geometric particle size was measured using a Mastersizer 3000 analyzer (Malvern Instruments Ltd., Worcestershire, UK) attached to a dry-dispersion accessory device (Aero S, Malvern Instruments). A pressure of 4 bars was used for the venturi dispenser with a feed rate of 90%. The refractive index of the sample was taken to be the average of the NIMs components multiplied by the percent (w/w) contained in the formulation: 70% w/w lactose (1.35), 20% w/w SPIONs (2.42), and 10% w/w fluorescent nanospheres (1.52) for a weighted average of 1.58. The results were expressed in terms of D_{v50} (volumetric median diameter). All samples were analyzed in triplicate and are expressed as mean ± standard deviation. The aerodynamic diameter of the NIMs was determined using a Next Generation Impactor (NGI) (model 170, MSP Corporation, Shoreview, MN). NIMs were insufflated into the NGI using the DP4 dry powder insufflator for rat (Penn Century, Inc., USA). The NGI was operated with a flow rate of 30L/min for 10 min. Particle deposition was determined by the gravimetric method.

Cell Culture. Human lung adenocarcinoma A549 cells (ATCC CCL-185) (American Type Tissue Culture, Manassas, Virginia, USA) were grown in Ham's F12K (Kaighn's) medium and supplemented with fetal bovine serum (FBS), 5% L-glutamine, 3% antimycotic, and 3% antibiotic (Life Technologies, Grand Island, NY, USA).

Cytotoxicity Studies. Confluent cells were exposed to dry powder NIMs containing doxorubicin (D-NIMs) and controls (doxorubicin solution, lactose solution, and SPIONs suspension). A549 cell viability and toxicity were tested using the CytoTox96 Non-Radioactive (3-(4,5-dimethylthiazol-2-yl)-5-(3-carboxymethoxyphenyl)-2-(4-sulfophenyl)-2H-tetrazolium (MTS) cell proliferation assay and the CytoTox96 Non-Radioactive lactate dehydrogenase (LDH) cytotoxicity assay, respectively. Briefly, D-NIMs were uniformly dispersed in F12K non-supplemented media with FBS at three different

DOI: 10.1021/acs.molpharmaceut.7b00532
Mol. Pharmaceutics 2017, 14, 4741−4750

doxorubicin concentrations: 0.16 μg/mL (low concentration), 1.6 μg/mL (medium concentration), and 16 μg/mL (high concentration) (referred to henceforth as low, medium, and high dose). The same media was used to generate free doxorubicin solutions with concentrations of 0.3 μg/mL (low), 3 μg/mL (medium), and 30 μg/mL (high). Controls consisting of lactose solution and SPIONs suspension were used at concentrations similar to those present in NIMs, as ratios from the spray dried feed solution were held constant relative to doxorubicin. Prior to exposure, A549 cells were washed with fresh media and 100 μL of the suspensions/solutions (D-NIMs; doxorubicin only; lactose; SPIONs).

CellTiter 96 Aqueous One Solution Reagent MTS assay (Promega, Madison, Wisconsin, USA) and CytoTox96 Non-Radioactive Assay LDH assay (Promega, Madison, Wisconsin, USA) were performed according to the manufacturer's instructions. In brief, at time periods of 1, 8, 24, 48 h post-exposure, 80 μL of cell culture supernatant was aspirated from each well and centrifuged at 300 × g for 10 min to settle any SPIONs or cells. MTS reagent was mixed with the cell culture supernatant at a ratio of 1:6 (MTS) or 1:2 (LDH), aliquoted into a black optical bottom 96-well plate and incubated at 37 °C and 5% CO_2 for 3 h (MTS) or 30 min (LDH). For LDH development, 50 μL of stop solution was added to each well. Absorbance was measured at a wavelength of 490 nm. Results were plotted as absorbance over time with respect to increasing amounts of doxorubicin present in the D-NIMs.

***In Vivo* Study Design.** Male Balb/c mice (6−8 weeks old; Jackson Laboratory, Sacramento, CA, USA) were used for the *in vivo* targeting studies. All rodents were housed in a temperature and light cycle controlled facility, and their care followed the guidelines of the National Institutes of Health and an approved Institutional Animal Care and Use Committee protocol (IACUC protocol number 11−100747-HSC). Mice were randomly assigned to 5 different groups with $n = 3$ per group: (1) untreated control mice; (2) mice administered NIMs dry powders magnetically-targeted to the left lung; (3) mice administered NIMs dry powders in the absence of magnetic targeting; (4) mice administered NIMs liquid suspensions magnetically-targeted to the left lung; (5) mice administered NIMs liquid suspensions in the absence of magnetic targeting. For the *in vivo* studies, doxorubicin in the NIMs was replaced with fluorescent nanoparticles as a drug surrogate to facilitate imaging.

Mice were anesthetized with a standard dose of xylazine/ketamine. A Dry Powder Insufflator for mouse (DP-4-M; Penn-Century Inc., Wyndmoor, PA, USA) was attached to a 1 mL disposable plastic syringe that was used to endotracheally administer the dry powder NIMs. Briefly, anesthetized mice were placed on their back on an intubation platform (Penn-Century Inc., Wyndmoor, PA, USA) and the tracheal opening was visualized by inserting a small animal laryngoscope (Model LS2; Penn-Century Inc.) [20] The insufflator delivery tube was inserted gently into the trachea of the animal, proximal to the carina, until the bend of the delivery tube was positioned at the incisors. Skin over the left lung of the mouse was carefully dissected without exposing the thoracic cavity[16] and a commercially available neodymium−iron−boron (NdFeB) permanent cylindrical magnet (grade N52, 22 mm long × 20 mm in diameter; Applied Magnets, Plano, TX) was centered 1 mm above the left lung to avoid contact with the tissue, with the edge of the magnet perpendicular to the upper region of the left lung (Figure 1C). Skin removal was performed to decrease the distance between the lung and the magnet, and maximize the magnetic targeting. The orientation of the magnet over the left lung was critical for the NIMs to be sufficiently attracted to the magnetic pole that was created by the externally-applied magnetic field. We had previously characterized the permanent magnet to have a magnetic field of 0.58 T.[17]

Approximately 2.0 mg of NIMs were loaded in the insufflator and administered using the plastic syringe with an air volume of 500 μL for a total of 10 puffs (10 actuations). Of the 2.0 mg loaded in the insufflator, 0.5 mg was delivered into the mouse lung based on the gravimetric analysis of the insufflator before and after dosing. A NIMs liquid suspension was administered using the MicroSprayer aerosolizer (1A-1C; Penn-Century) for mouse and was attached to a hand-operated, high-pressure syringe (FMJ-250; Penn-Century).[21] Mice were endotracheally intubated and 50 μL of saline containing 0.5 mg of the NIMs dry powder (w/v solids; containing equivalent amounts of the fluorescent dye and SPIONs) was administered directly into the airways with the MicroSprayer. Control mice were treated similarly using the dry powder NIMs and liquid suspension in the absence of magnetic-field-dependent targeting. Mice were sacrificed immediately after pulmonary delivery; lungs and trachea were removed en bloc, separated (Figure 1D), and fluorescence and iron deposition were quantified in the respective tissues.

Fluorescence Quantification. NIMs dry powder and NIMs suspension were administered endotracheally and targeted to the left lung in the presence of a permanent magnet. Individual lung lobes and trachea were excised and imaged immediately for fluorescence (λ_{ex} = 660 nm and λ_{em} = 680 nm) with an exposure time of 10 s using a Caliper IVIS Lumina II imaging system (Caliper Life Sciences). A region of interest (ROI) was drawn around the trachea, left lung, right lung, and background. The ROI area was kept constant at 2.5 cm^2 and fluorescence was expressed as units of average radiance efficiency (RE) $(p/sec/cm^2/sr)/(\mu W/cm^2)$.[22]

Fluorescence calculations.

$$\%\text{Targeting} = \frac{FI_{individual}}{FI_{sum}} \times 100$$

$$\text{Targeting Efficiency L:R Ratio} = \frac{\%FI_{Left\ Lung}}{\%FI_{Right\ Lung}} \quad (1)$$

Percent targeting was calculated by determining ratios of the fluorescence intensity ($FI_{individual}$) of ROIs from individual tissue (e.g., left lung) in the numerator, divided by the sum of fluorescence intensity (FI_{sum}) of the three ROI areas (trachea, left lung, and right lung) in the denominator (eq 1), and multiplied by 100. Targeting efficiency L:R ratio was calculated using the percent targeting of the left lung in the numerator, divided by the percent targeting of the right lung in the denominator.

Iron Quantification. Inductively coupled plasma optical emission spectroscopy (ICP-OES) was used to measure ferrous iron content in the mouse lungs and trachea. Briefly, tissue was digested with 0.5 mL nitric acid (HNO_3) at 105 °C for 1 h and vortexed until completely dissolved (protocol modified from Niazi et al.[23]). After cooling, the samples were brought up to a known volume with Milli-Q water. Samples were analyzed with a PerkinElmer Optima 4300 DV ICP-OES. The recommended wavelength for iron was used, Fe (II)-λ-259.939 nm. A five-

DOI: 10.1021/acs.molpharmaceut.7b00532
Mol. Pharmaceutics 2017, 14, 4741−4750

point calibration standard range was used that ranged from 0.1 to 25 ppm (mg/L). Endogenous iron was analyzed from the lungs of untreated mice ($n = 3$), and the average of these values was subtracted from the treated mice. Calibration and instrument verification samples were incorporated before and after analyzing the samples, as well as periodically throughout the measurements.

Iron calculations.

$$\%\text{Targeting} = \frac{[\text{Iron}]_{\text{individual}}}{[\text{Iron}]_{\text{sum}}} \times 100$$

$$\text{Targeting Efficiency L:R Ratio} = \frac{\%[\text{Iron}]_{\text{Left Lung}}}{\%[\text{Iron}]_{\text{Right Lung}}} \quad (2)$$

Targeting efficiency ratio was calculated by determining ratios of the iron content from individual tissue (e.g., left lung) in the numerator, divided by the sum of the total iron content for all three tissues (trachea, left lung, and right lung) in the denominator (eq 2), and multiplied by 100. Targeting efficiency L:R ratio was calculated using the percent targeting of the left lung in the numerator, divided by the percent targeting of the right lung in the denominator.

Dye and Iron Targeting Corroboration.

Fluorescence and iron differentials.

$$\text{Fluorescence differential} = \text{FI}_{\text{Left Lung}} - \text{FI}_{\text{Right Lung}}$$

$$\text{Iron differential} = [\text{Iron}]_{\text{Left Lung}} - [\text{Iron}]_{\text{Right Lung}} \quad (3)$$

Targeting of dye and iron was corroborated by calculating the differential between the fluorescence (relative efficiency) or iron concentrations in left lung compared to the right (eq 3).

Statistical Analysis. All statistical analysis was performed using GraphPad Prism statistical software (GraphPad Software, San Diego, CA). Paired t tests with Bonferroni correction were used to compare two or more groups of independent data. The difference between variants was considered significant if $p < .05$. For comparisons of more than two an ordinary one-way ANOVA was used to determine significance, with Tukey's multiple comparisons and a Brown-Forsythe test was used to compare variances. If more than two variables were taken into account, a two-way ANOVA was employed with Sidak's multiple comparison. A post-hoc power calculation was performed using the free program G*power (Dusseldorf, Germany).[24,25] For *in vivo* animal experiments with equivalent sample sizes and an effect size of n = 3, the power was calculated to be >.95.

RESULTS

Dry Powder NIMs Formulation and Characterization. Dry powder NIMs for pulmonary administration were prepared as described previously using lactose as the bulking agent.[17,26] NIMs were characterized for aerodynamic and geometric diameters, surface charge of the SPIONs, morphology, magnetic behavior, iron content, and drug loading (Table 1).[17] For this study, doxorubicin, a common chemotherapeutic agent with demonstrated activity against lung cancer, was used. NIMs with doxorubicin will be referred to as D-NIMs.

***In Vitro* Evaluation of Chemotherapeutic Efficacy.** To assess whether the doxorubicin in D-NIMs retained its cytotoxicity (and therefore its therapeutic effect) after spray drying, a MTS assay was utilized to measure cell viability of lung adenocarcinoma cells after D-NIMs exposure. We hypothesized that D-NIMs would quickly release the doxorubicin and would have similar or increased cytotoxicity compared to free doxorubicin in A549 cells. The left panel of Figure 2 compares A549 cells treated with D-NIMs, as well as controls consisting of spray-dried lactose, SPIONs alone, and free doxorubicin solution. A549 cells were exposed to low, medium, and high doses of free doxorubicin solution or D-NIMs for a total of 48 h (Figure 2). It is important to note that the concentration of doxorubicin was approximately doubled in the free doxorubicin solution control group compared to the D-NIMs dry powder group at all three doses. The low concentration of free doxorubicin solution (0.03 μg) or D-NIMs (0.016 μg) showed minimal cytotoxicity, and cells were as viable as untreated A549 cells after 48 h of exposure (Figure 2A, MTS panel). However, medium and high doses of doxorubicin solution and D-NIMs were toxic to adenocarcinoma cells compared to SPIONs and lactose controls. Importantly, at both medium and high doses, no significant differences were seen between the free doxorubicin and D-NIMs groups ((67 ± 1.67)% and (58 ± 0.51)% respectively), despite D-NIMs containing doxorubicin at nearly half the concentration of the free doxorubicin group (Figure 2C, MTS panel).

The LDH assay was used to confirm D-NIMs cytotoxicity to A549 adenocarcinoma cells. The amount of LDH released is proportional to the number of cells damaged or lysed with increased absorbance signifying low cell viability.[27,28] The right panel of Figure 2 compares cells treated with free doxorubicin solution to D-NIMs. Neither spray-dried lactose nor SPIONs alone were cytotoxic to A549 lung adenocarcinoma cells (Figure 2A-C).

However, A549 cells exposed to a low concentration of D-NIMs (144.5 ± 20.82)% had equal damage to cells treated with free doxorubicin (111.3 ± 0.653)% after 48 h of exposure, despite having less doxorubicin (Figure 2A, LDH panel). Furthermore, medium and high doses of D-NIMs followed the same trend, showing equal toxicity to that of free doxorubicin (Figure 2B and C, LDH panel).

Magnetic-Field-Dependent *in Vivo* Targeting. To assess the targeting capability of dry powder NIMs, SPIONs were spray dried with fluorescent nanospheres (as a drug surrogate) and were endotracheally delivered in the presence of an external permanent magnet to the left lung of healthy, anesthetized mice (Figure 1C). Fluorescence associated with NIMs was quantified in the mouse trachea, and the left and

Table 1. Characterization of SPIONs and NIMs[a]

SPIONs		NIMs
average radius	56 ± 6 nm	concentration (w/w)
density	2.5 g/cm^3	1.6% doxorubicin
zeta potential	−49 mV	10.6% Fe_3O_4
		laser diffraction 1.6 μm
		next generation impaction
		MMAD[b] 3.27 μm
		FPF[c] > 90%
		GSD[d] ± 1.69

[a]For NIMs dry powder. For more details on the NIMs powder preparation and characterization consult McBride et al.[17] [b]Mass median aerodynamic diameter (MMAD). [c]Fine particle fraction (FPF). [d]Geometric standard deviation (GSD).

DOI: 10.1021/acs.molpharmaceut.7b00532
Mol. Pharmaceutics 2017, 14, 4741−4750

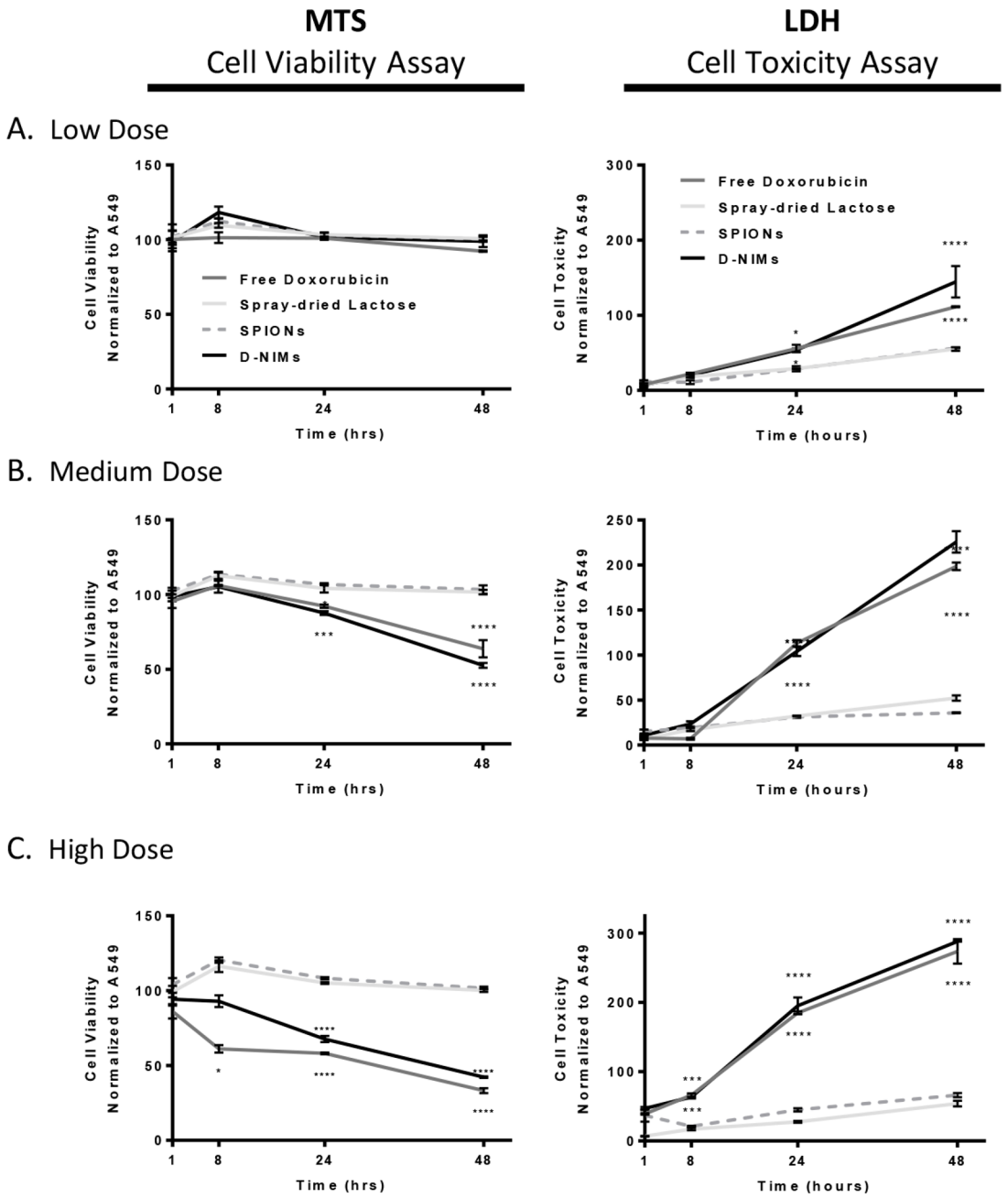

Figure 2. MTS viability and LDH cytotoxicity assay of A549 cells exposed to doxorubicin-loaded NIMs. MTS (left panel) and LDH (right panel) assay measuring viability and cytotoxicity, respectively, of A549 lung adenocarcinoma cells after 48 h of exposure to (A) low dose of D-NIMs compared to free doxorubicin (1 μg NIMs containing 0.016 μg doxorubicin compared to 0.03 μg free doxorubicin), (B) medium dose of D-NIMs compared to free doxorubicin (10 μg NIMs containing 0.16 μg doxorubicin compared to 0.3 μg free doxorubicin), and (C) high dose of D-NIMs compared to free doxorubicin (100 μg NIMs containing 1.6 μg doxorubicin compared to 3.0 μg free doxorubicin). Free doxorubicin control (dark gray), spray-dried lactose control (light gray), SPIONs control (dashed gray), D-NIMs (black); for both MTS and LDH panels. Lactose and SPIONs controls were used at the ratios from the spray-dried feed solution and were held constant relative to doxorubicin. A two-way ANOVA with Sidak's multiple comparison test was used to determine statistical significance. *p <.05; **p <.01, ***p <.001, ****p <.0001; data shown with standard error of the mean (SEM) and n = 3.

right lung; this data was used to calculate the targeting efficiency of NIMs to specific regions of the respiratory tract (Figure 3A–C).

In the presence of magnetic targeting, NIMs powder had significantly higher fluorescence units of radiance efficiency (RE) detected in the left lung ((44.5 ± 2.3)% RE) compared to the right lung ((14.33 ± 5.6)% RE; p < 0.01) (Figures 3D and S1A). This represents more than 3-fold higher total fluorescence in the left lung, demonstrating significant targeting to the magnetized lung. To corroborate the separation of SPIONs and the drug surrogate from liquid formulations observed by Dames et al.,[16] we delivered a liquid suspension of NIMs by the pulmonary route. Targeting of the fluorescent dye to the left lung was nearly non-existent, with fluorescence efficiency in the left magnetized lung ((46.3 ± 6.9)% RE) nearly equal to that seen in the right lung ((39.2 ± 2.6)% RE (Figures 3D and S1B). When dry powder NIMs were administered into the lungs of mice in the absence of magnetic

DOI: 10.1021/acs.molpharmaceut.7b00532
Mol. Pharmaceutics 2017, 14, 4741–4750

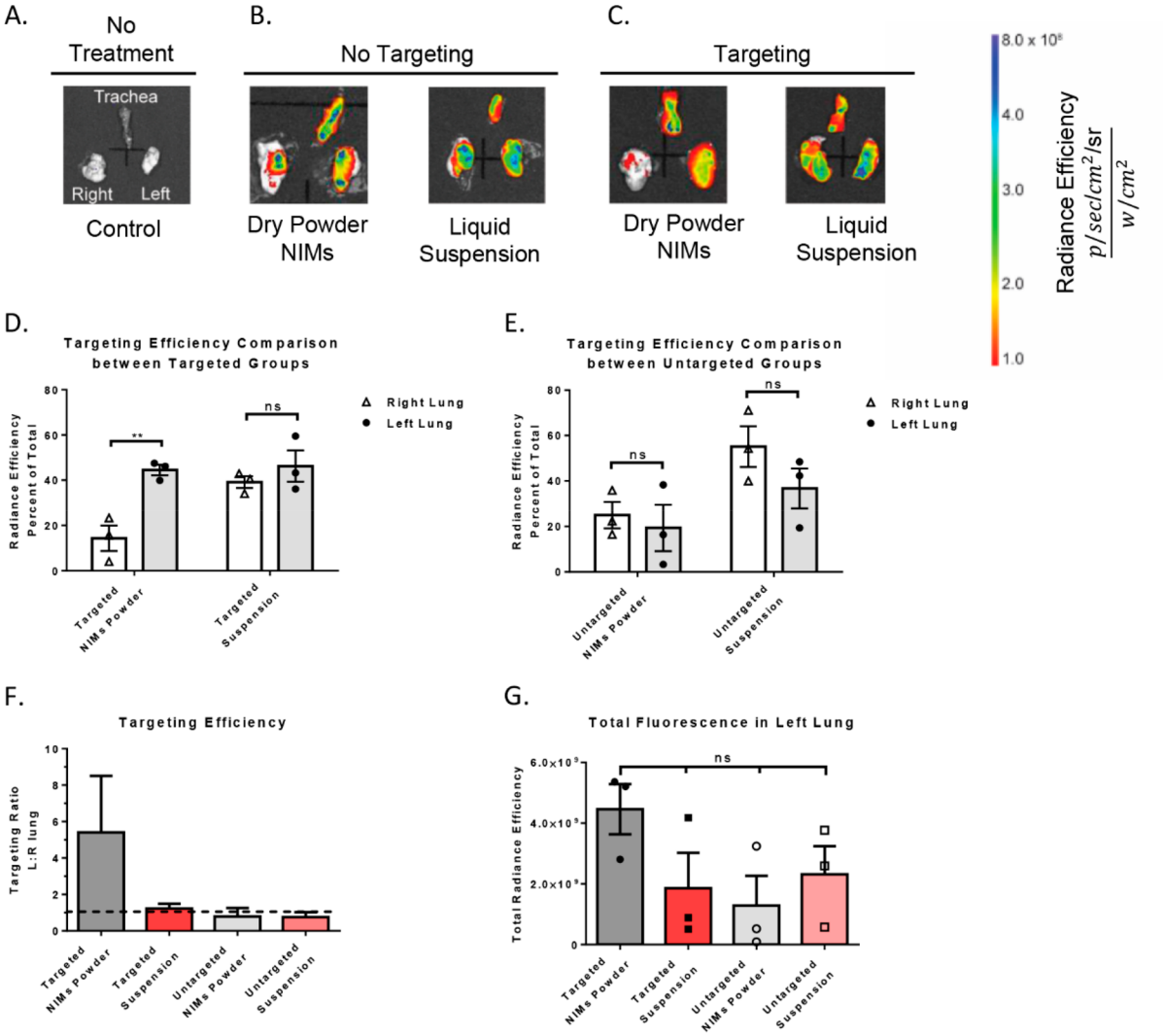

Figure 3. Fluorescence quantification in murine lungs after magnetic-field-dependent targeting. (A) Untreated control, no fluorescence is observed in lungs or trachea (n = 1). The trachea (upper half of image), the right lung (left side of image), and the left lung (right side of image) are shown. (B) No targeting controls: NIMs dry powder and liquid suspension in the absence of magnetic targeting (n = 3; representative images shown). (C) Targeted treatment groups: NIMs dry powder and liquid suspension in the presence of magnetic targeting (n = 3; representative images shown). (D,E) Comparison of targeting efficiency (measured as radiance efficiency, graphed as percent of total) of NIMs dry powder and liquid suspension in left (targeted) and right lungs (untargeted) in the (D) presence and (E) absence of magnetic targeting. (F) Targeting efficiency ratio between the left (targeted) and the right (untargeted) lung in the presence and absence of magnetic-field-dependent targeting. The dashed line represents equal fluorescence in the left and right lung. Any fluorescence above the dashed line shows targeting to magnetized left lung. (G) Fluorescence (in total radiance efficiency) quantified in the left targeted lung after delivery of NIMs dry powder and liquid suspension (in the presence and absence of magnetic targeting). A two-way ANOVA with Sidak's multiple comparison test (for D and E) or a one-way ANOVA with Tukey's multiple comparison post-test (for G) was used to determine statistical significance. *p <.05; **p <.01; ns = not significant; data shown with standard error of the mean (SEM) and n = 3.

targeting, fluorescence intensity was similar in the left ((19.33 ± 10.2)%RE) and right lung ((24.9 ± 5.7)%RE) (Figures 3E and S1C). NIMs suspension in the absence of magnetic targeting gave similar results, with ((36.7 ± 8.8)% RE) in the left lung and ((55.1 ± 9.0)% RE) in the right lung (Figures 3E and S1D). Control animals that were not administered NIMs exhibited no background fluorescence in either the left or right lung (Figure 3A). Importantly, targeting efficiency, which is assessed by calculating the ratio of the fluorescence intensity in the left to right lung, showed targeting only with the dry powder NIMs (in the presence of a magnetic field) (Figure 3F). All other treatment groups showed a ratio close to one, suggesting similar fluorescence intensity and targeting in both the right and left lung.

The dose of powder delivered into the lung using the insufflator can vary based on the powder properties as well as the air volume used for powder dispersion. Approximately 2.0 mg of NIMs was loaded into the insufflator and 0.4−0.6 mg of NIMs were delivered to the respiratory tract of each mouse, based on the weight of the insufflator before and after dosing. Interestingly, total fluorescence in the left lung was not significantly different among the groups that were administered NIMs (dry powders and liquid suspensions), suggesting that the actual amount of dye in the left lung did not change significantly between groups (Figure 3G). However, significant differences are apparent in the assessment of dye targeting to the left lung out of the total lung fluorescence (Figure 3F,G).

DOI: 10.1021/acs.molpharmaceut.7b00532
Mol. Pharmaceutics 2017, 14, 4741−4750

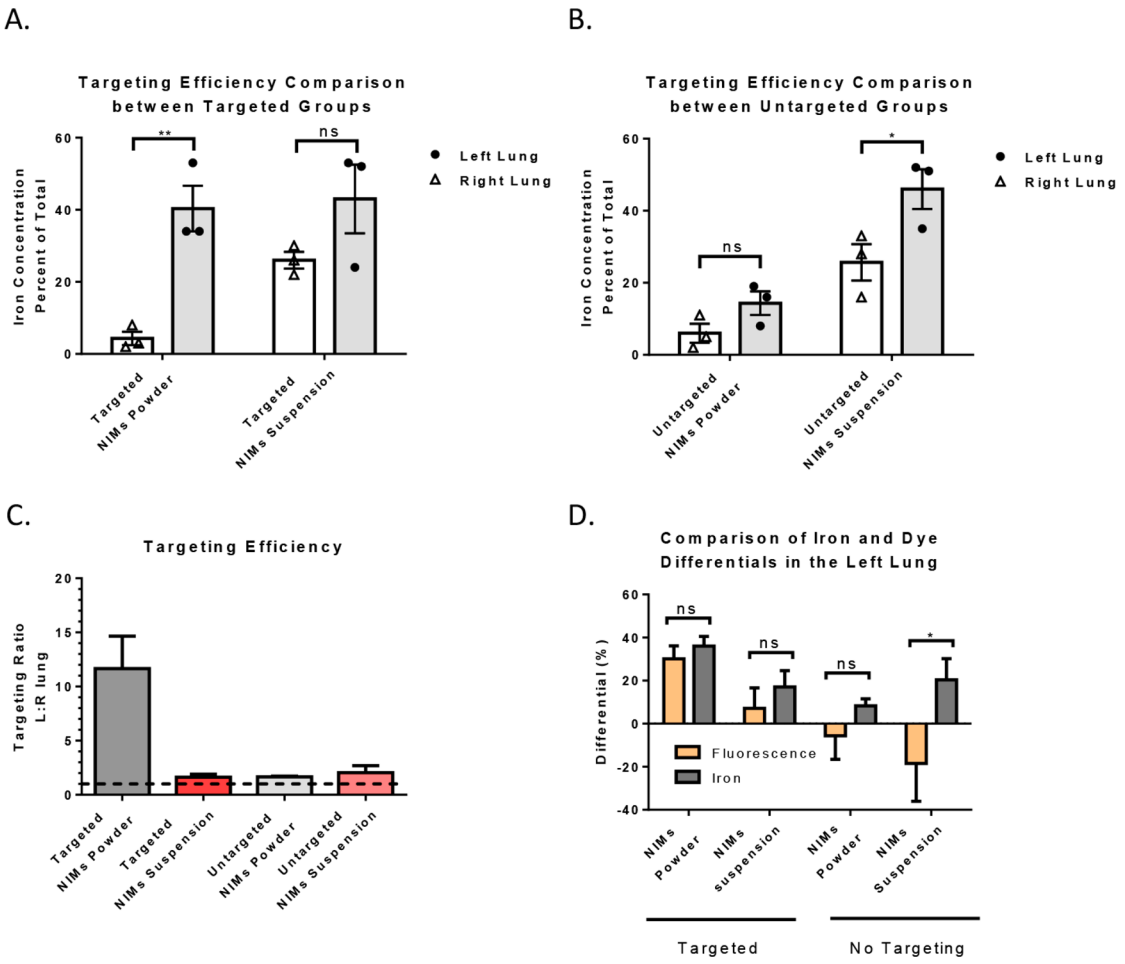

Figure 4. Iron quantification of magnetic targeting and corroboration of iron and dye components from NIMs. Comparison of targeting efficiency (measured as iron concentration, graphed as percent of total) of NIMs dry powder and liquid suspension in left (targeted) and right lungs (untargeted): (A) in the presence and (B) in the absence of magnetic targeting. (C) Comparison of iron targeting efficacy between vehicles in the presence and absence of targeting. Dashed line describes equal iron in left and right lung. Iron above shows targeting to left lung and below shows anti-targeting to right lung. (D) Comparison of fluorescence and iron differentials to the left lung (see eq 3) in the presence and absence of magnetic targeting of NIMs powder and liquid suspension. A two-way ANOVA with Sidak's multiple comparison test (for A, B, and D) was used to determine statistical significance. *p <.05; **p <.01; ns = not significant; data shown with standard error of the mean (SEM) and n = 3.

Efficacy of Magnetic-Field-Dependent Targeting as Determined by Iron Quantification. To confirm the targeting of NIMs seen using fluorescence quantification, we used inductively coupled plasma optical emission spectroscopy (ICP-OES) to quantify SPIONs in the lungs and trachea after magnetic-field-dependent targeting of the NIMs.[29−32] ICP-OES does not distinguish between endogenous iron present in the lung and exogenous sources of iron. Therefore, we compensated lung samples by quantifying and subtracting endogenous iron in left and right lung tissue, as well as in the trachea. The left lung had an average endogenous iron concentration of 156.0 ± 3.1 μg/g, the right lung 135.0 ± 16.3 μg/g iron, and the trachea 88.2 ± 11.4 μg/g iron (Figure 4A, B; data graphed as % iron in left and right lung.)

In the case of NIMs powder targeted to the left lung with a permanent external magnet, more iron was quantified in the left lung ((40.3 ± 6.3)% total iron) than the right lung ((4.3 ± 1.9)% total iron) (p <.01, n = 3). This 10-fold increase in SPIONs deposition in the left lung suggests that dry powder NIMs were significantly targeted to the left lung over the right lung (Figures 4A and S2A). In contrast, the NIMs liquid suspension did not show significant targeting of SPIONs to the magnetized lung; the left lung ((43.0 ± 9.5)% total iron) showed no statistical difference from the right lung ((26.0 ± 2.3)% total iron) (Figures 4A and S2B). In the absence of a magnetic field, dry powder NIMs showed no difference in iron levels between the right and left lung, with ((14.3 ± 3.3)% total iron) in the left lung and ((6.0 ± 2.6)% total iron) in the right (Figures 4B and S2C). However, we saw differential deposition of iron in the lung lobes in the NIMs liquid suspension without magnetic targeting, with ((46.0 ± 5.5)% total iron) in the left lung and ((25.6 ± 5.0)% total iron) in the right (p <.05, n = 3) (Figures 4B and S2D). Importantly, the targeting efficiency, measured by calculating the ratio of iron in the left lung (magnetized) over the right lung (non-magnetized), showed targeting only in the dry powder NIMs group (Figure 4C).

Corroboration of NIMs Targeting by Comparing Targeting Differentials for Iron and Dye. To compare whether the targeting efficiencies of the fluorescent dye and iron were similar within each treatment group, we calculated the fluorescence and iron differentials between the right and left lung (Figure 4D). Similar targeting differentials for the dry powder NIMs would suggest that the dye and SPIONs were delivered as a single entity to the target region. However,

DOI: 10.1021/acs.molpharmaceut.7b00532
Mol. Pharmaceutics 2017, 14, 4741−4750

differences in fluorescence and iron differentials may suggest separation of SPIONs and the dye during pulmonary administration, as seen by Dames et al. using liquid suspensions.[16]

When comparing fluorescence and iron levels in the left and right lung, equal differentials were seen in the dry powder NIMs group in the presence of magnetic targeting (average differential of fluorescence (30 ± 6)%; average differential of iron (36 ± 5)% (Figure 4D). This suggests that dry powder NIMs were delivered to the lung as intact microparticles. Similarly, the NIMs suspension did not show any significant differences in fluorescence ((7.1 ± 9.5)% to left lung) and iron ((17.0 ± 7.6)% to the left lung) differentials; however, the large variability in the differentials of fluorescence and iron suggest some pre-separation of iron and the dye during pulmonary administration. Furthermore, in the absence of magnetic targeting, iron and fluorescence differentials were significantly different for the NIMs suspension and dry powder groups (suspension: average differential of fluorescence (−18.4 ± 17.6)% to left lung; iron accumulation of NIMs, average differential of iron (20.3 ± 9.9)% to left lung); (dry powder: average differential of fluorescence (−5.6 ± 10.9)% to left lung; iron accumulation of NIMs, average differential of iron (8.3 ± 3.1)% to left lung)) (Figure 4D).

DISCUSSION

Chemotherapy for lung cancer by the pulmonary route has recently shown promise in a Phase I/II study; however, its effectiveness was limited due to pulmonary dose-limiting toxicity to healthy tissues.[11] Therefore, the ultimate goal of our NIMs drug delivery platform is to carry high payloads of chemotherapeutic agents to specific regions of the lung, thereby minimizing toxicity to healthy lung tissue and maximizing chemotherapeutic effect in the tumor microenvironment. The concept of using SPIONs for targeted pulmonary delivery have been proposed by us and others, previously.[16,17,33,34] Dames and colleagues showed the pulmonary targeting of a drug surrogate suspended in a liquid with SPIONs using an external permanent magnet in healthy mice.[16] This study was the first to use iron oxide nanoparticles to target a drug surrogate to an externally magnetized lung lobe. Higher iron deposition and lower drug surrogate in the magnetized lung lobe suggested that the liquid suspension carrying the drug surrogate and SPIONs separated during aerosolization and pulmonary administration before reaching the targeted lung region.[16] SPIONs were attracted to the external magnet placed over the targeted lung lobe, whereas the drug surrogate traveled the natural trajectory of the aerosol in the respiratory tract. Our laboratory had previously confirmed the separation effect of SPIONs and dye in a liquid suspension using a glass model of the human trachea.[17]

To address this issue, dry powder NIMs were designed for pulmonary administration, using lactose as a binding excipient and SPIONs to externally target the drug payload to one lung lobe versus the other (Table 1).[17,35,36] Previously, a study by Xie and colleagues showed the feasibility of targeting aerosols of dried fluorescein-coated iron nanoparticle aggregates using computational assessment of lung and blood deposition.[33] Pulmonary delivery requires particles to be in the 1−5 μm range with larger particles impacting the oropharyngeal region and smaller particles being exhaled.[17] Lactose has been approved by the FDA for pulmonary delivery and was used as a binding agent for NIMs [35]. The lactose matrix decreases the dissolution time of NIMs after pulmonary delivery due to the solubility of lactose in the lung fluid. SPIONs were incorporated for their superparamagnetic behavior, which we demonstrated in dry powder NIMs based on zero coercivity.[17]

In vitro A549 adenocarcinoma exposure studies were performed to ensure that doxorubicin-loaded in dry powder NIMs maintained its anti-cancer effects after the spray drying process (Figure 2). Interestingly, D-NIMs showed as much or more therapeutic cytotoxicity as free doxorubicin solution, despite having a lower total doxorubicin concentration (Figure 2B,C). It suggests that the doxorubicin encapsulated within NIMs may achieve the therapeutic effect with half the dose of doxorubicin when it is not encapsulated in NIMs. We speculate that the increased toxicity of D-NIMs is a synergistic effect of increased cellular uptake of SPIONs and reactive oxygen species production, which may enhance the cytotoxic effects of doxorubicin.[28,37] We did not expect lactose to show any toxicity when exposed to A549 cells since it is a FDA approved excipient for dry powders used in pulmonary delivery.[38] Similarly, the safety of SPIONs has been demonstrated in humans when used as a diagnostic agent for imaging.[28] Furthermore, SPIONs were shown to be cleared by alveolar macrophages after pulmonary exposure.[39,40] Prijic et al., showed the safety and biocompatibility of SPIONs, exposing mouse fibroblasts and human melanoma cells to different concentrations of SPIONs (10−200 μg/mL).[41] These authors also showed that there were no cytotoxic effects associated with the external magnetic field generated by the permanent NdFeB magnet.

The targeting capability of NIMs dry powder compared to a liquid suspension was shown using a fluorescent dye. Dry powder NIMs showed significantly higher targeting of both fluorescence (drug surrogate) and iron than the liquid NIMs suspension, in the presence of an external magnet (Figures 3 and 4). Furthermore, the targeting efficacy differentials for fluorescence and iron were similar for NIMs powder suggesting that the separation of the dye and SPIONs did not occur during aerosolization and pulmonary delivery (Figure 4D). These data taken together suggest that dry powder NIMs can be targeted to specific regions of the lung in a preclinical model, and the dry powder particles do not separate during aerosolization unlike liquid formulations containing SPIONs.[16]

We also observed significant deposition of iron and fluorescent dye in the trachea of mice that were administered dry powder NIMs compared to the liquid suspension (Figures S1 and S2). Tonnis et al. recently showed that the DP-4 M insufflator delivery device leads to significant powder deposition in the trachea.[42] Furthermore, Hoppentocht et al. and others have observed that 200 μL air volume, as recommended by the device manufacturers, did not provide adequate powder aerosolization and subsequent delivery in the lungs of mice.[43,44] We confirmed this observation and showed that the insufflator required a larger air volume of ∼500 μL for adequate NIMs dispersion into the murine lung. However, we speculate that the turbulent airstream generated by the syringe due to this larger air volume may have led to the significantly higher powder deposition in the trachea due to inertial impaction.[44] We suspect while both dry powder NIMs and the liquid suspension impacted the tracheal walls, the liquid suspension flowed down the tracheal wall into the initial branches of the lung. This may have possibly led to less fluorescent dye and SPIONs observed in the trachea from the

DOI: 10.1021/acs.molpharmaceut.7b00532
Mol. Pharmaceutics 2017, 14, 4741−4750

NIMs liquid suspension, as well as the apparent deposition of the iron in the unmagnetized lung lobes (Figure 4B).

Using dry powder NIMs as a targeting strategy to specific regions of the lungs of humans has some significant challenges ahead. Since the gradient of the magnetic force generated by an external magnet decreases exponentially with distance, the main limitation of this delivery mechanism relates to the strength of the magnetic field that can be applied to the patient to obtain the necessary magnetic gradient in the respiratory tract. This may be further exacerbated by differences in airway geometry and tumor location in the respiratory tract, which varies between patients. This treatment modality may require a "personalized medicine". Electromagnets or the substantial magnetic field gradients that are used in human MRI imaging may be able to overcome the rapid fall in magnetic field strength over distance, however further studies are required to validate their safety.[45] However, spray drying offers the flexibility to modulate the amount of chemotherapeutic agent or SPIONs that can be loaded in NIMs beyond what is proposed in this study; by increasing the SPIONs concentration in NIMs, they can be influenced by externally generated magnetic fields to a greater extent. In addition, the ability to manipulate the ratio of chemotherapeutic agent to SPIONs in NIMs could diminish toxicity or improve anti-tumor effects.

Although magnetic targeting of drugs using NIMs dry powder has the potential utility in many respiratory diseases, localized tumors will benefit the most from this targeting mechanism. Future studies will include targeting dry powder NIMs containing a single or a combination of chemotherapeutic agents in an orthotopic lung cancer mouse model recently developed in our laboratory.[46] This study would demonstrate the ability of dry powder NIMs to cause tumor regression when delivered by the pulmonary route. Delivery of magnetically-responsive NIMs to specific regions of the lung has the potential to be the first non-invasive therapeutic approach for the treatment of non-metastasized solid lung tumors.

■ ASSOCIATED CONTENT

Supporting Information

The Supporting Information is available free of charge on the ACS Publications website at DOI: 10.1021/acs.molpharmaceut.7b00532.

Effect of magnetic-field-dependent targeting by fluorescence quantification and by iron (SPION) quantification in murine lungs (PDF)

■ AUTHOR INFORMATION

Corresponding Author

*Telephone: (505) 272-2569; E-mail: pmuttil@salud.unm.edu.

ORCID

Nitesh K. Kunda: 0000-0002-3063-0375

Pavan Muttil: 0000-0001-7636-8141

Notes

The authors declare no competing financial interest.

■ ACKNOWLEDGMENTS

We acknowledge Dr. Mehdi Ali of the Earth and Planetary Sciences Department at UNM for his technical assistance with ICP-OES. This work was supported in part by the Dedicated Health Research Funds from the University of New Mexico, School of Medicine. D.N.P. was supported by the Bill and Melinda Gates Grand Challenge Exploration (No OPP1061393) and UNM IDIP T32 training grant (T32-A1007538, P.I. – M. Ozbun) and the start-up funds for Dr. Pavan Muttil from the UNM College of Pharmacy.

■ ABBREVIATIONS

nano-in-microparticles, NIMs; superparamagnetic iron oxide nanoparticles, SPIONs; next generation impactor, NGI; NIMs containing doxorubicin, D-NIMs; average radiance efficiency, RE; inductively coupled plasma optical emission spectroscopy, ICP-OES; mass median aerodynamic diameter, MMAD; fine particle fraction, FPF; geometric standard deviation, GSD

■ REFERENCES

(1) American Cancer Society Cancer Facts & Figures 2016. *Cancer Facts Fig.*; 2016; Vol. *2016*, pp 1–9.

(2) Siegel, R.; Ma, J.; Zou, Z.; Jemal, A. Cancer Statistics. *Ca-Cancer J. Clin.* **2014**, *64* (1), 9–29.

(3) IARC *World Cancer Report*; Stewart, B. W., Wild, C. P., Eds.; 2014

(4) Patton, J. S.; Byron, P. R. Inhaling Medicines: Delivering Drugs to the Body through the Lungs. *Nat. Rev. Drug Discovery* **2007**, *6* (1), 67–74.

(5) Hickey, A. J. Back to the Future: Inhaled Drug Products. *J. Pharm. Sci.* **2013**, *102* (4), 1165–1172.

(6) Chan, H. K.; Chew, N. Y. K. Novel Alternative Methods for the Delivery of Drugs for the Treatment of Asthma. *Adv. Drug Delivery Rev.* **2003**, *55* (7), 793–805.

(7) Acerbi, D.; Brambilla, G.; Kottakis, I. Advances in Asthma and COPD Management: Delivering CFC-Free Inhaled Therapy Using Modulite® Technology. *Pulm. Pharmacol. Ther.* **2007**, *20* (3), 290–303.

(8) Garcia-Contreras, L.; Hickey, A. J. Aerosol Treatment of Cystic Fibrosis. *Crit. Rev. Ther. Drug Carrier Syst.* **2003**, *20* (5), 317–356.

(9) Sakagami, M. Systemic Delivery of Biotherapeutics through the Lung: Opportunities and Challenges for Improved Lung Absorption. *Ther. Delivery* **2013**, *4* (12), 1511–1525.

(10) Otterson, G. A.; Villalona-Calero, M. A.; Sharma, S.; Kris, M. G.; Imondi, A.; Gerber, M.; White, D. A.; Ratain, M. J.; Schiller, J. H.; Sandler, A.; Kraut, M.; Mani, S.; Murren, J. R. Phase I Study of Inhaled Doxorubicin for Patients with Metastatic Tumors to the Lungs. *Clin. Cancer Res.* **2007**, *13* (4), 1246–1252.

(11) Otterson, G. A.; Villalona-Calero, M. A.; Hicks, W.; Pan, X.; Ellerton, J. A.; Gettinger, S. N.; Murren, J. R. Phase I/II Study of Inhaled Doxorubicin Combined with Platinum-Based Therapy for Advanced Non-Small Cell Lung Cancer. *Clin. Cancer Res.* **2010**, *16* (8), 2466–2473.

(12) Zarogoulidis, P.; Darwiche, K.; Krauss, L.; Huang, H.; Zachariadis, G. A.; Katsavou, A.; Hohenforst-Schmidt, W.; Papaiwannou, A.; Vogl, T. J.; Freitag, L.; Stamatis, G.; Zarogoulidis, K. Inhaled Cisplatin Deposition and Distribution in Lymph Nodes in Stage II Lung Cancer Patients. *Future Oncol.* **2013**, *9* (9), 1307–1313.

(13) Zarogoulidis, P.; Darwiche, K.; Kalamaras, G.; Huang, H.; Hohenforst-Schmidt, W.; Zarogoulidis, K. Targeted versus Chrono-Targeted Chemotherapy for Inhaled Chemotherapy in Non-Small Cell Lung Cancer. *Transl. lung cancer Res.* **2013**, *2* (1), E17–E22.

(14) Veronesi, G.; Szabo, E.; DeCensi, A.; Guerrieri-Gonzaga, A.; Bellomi, M.; Radice, D.; Ferretti, S.; Pelosi, G.; Lazzeroni, M.; Serrano, D.; Lippman, S. M.; Spaggiari, L.; Nardi-Pantoli, A.; Harari, S.; Varricchio, C.; Bonanni, B. Randomized Phase II Trial of Inhaled Budesonide versus Placebo in High-Risk Individuals with CT Screen-Detected Lung Nodules. *Cancer Prev. Res.* **2011**, *4* (1), 34–42.

(15) Chou, A. J.; Gupta, R.; Bell, M. D.; Riewe, K. O.; Meyers, P. A.; Gorlick, R. Inhaled Lipid Cisplatin (ILC) in the Treatment of Patients with Relapsed/progressive Osteosarcoma Metastatic to the Lung. Pediatr. *Blood Cancer* **2013**, *60* (4), 580–586.

DOI: 10.1021/acs.molpharmaceut.7b00532
Mol. Pharmaceutics 2017, 14, 4741–4750

(16) Dames, P.; Gleich, B.; Flemmer, A.; Hajek, K.; Seidl, N.; Wiekhorst, F.; Eberbeck, D.; Bittmann, I.; Bergemann, C.; Weyh, T.; Trahms, L.; Rosenecker, J.; Rudolph, C. Targeted Delivery of Magnetic Aerosol Droplets to the Lung. *Nat. Nanotechnol.* **2007**, *2* (8), 495−499.
(17) McBride, A. A.; Price, D. N.; Lamoureux, L. R.; Elmaoued, A. A.; Vargas, J. M.; Adolphi, N. L.; Muttil, P. Preparation and Characterization of Novel Magnetic Nano-in-Microparticles for Site-Specific Pulmonary Drug Delivery. *Mol. Pharmaceutics* **2013**, *10* (10), 3574−3581.
(18) Roa, W. H.; Azarmi, S.; Al-Hallak, M. H. D. K.; Finlay, W. H.; Magliocco, A. M.; Löbenberg, R. Inhalable Nanoparticles, a Non-Invasive Approach to Treat Lung Cancer in a Mouse Model. *J. Controlled Release* **2011**, *150* (1), 49−55.
(19) Gagnadoux, F.; Hureaux, J.; Vecellio, L.; Urban, T.; Le Pape, A.; Valo, I.; Montharu, J.; Leblond, V.; Boisdron-Celle, M.; Lerondel, S.; Majoral, C.; Diot, P.; Racineux, J. L.; Lemarie, E. Aerosolized Chemotherapy. *J. Aerosol Med. Pulm. Drug Delivery* **2008**, *21* (1), 61−70.
(20) Morello, M.; Krone, C. L.; Dickerson, S.; Howerth, E.; Germishuizen, W. A.; Wong, Y.-L. L.; Edwards, D.; Bloom, B. R.; Hondalus, M. K. Dry-Powder Pulmonary Insufflation in the Mouse for Application to Vaccine or Drug Studies. *Tuberculosis (Oxford, U. K.)* **2009**, *89* (5), 371−377.
(21) Price, D. N.; Kusewitt, D. F.; Lino, C. A.; McBride, A. A.; Muttil, P. Oral Tolerance to Environmental Mycobacteria Interferes with Intradermal, but Not Pulmonary, Immunization against Tuberculosis. *PLoS Pathog.* **2016**, *12* (5), e1005614.
(22) Ally, J.; Martin, B.; Behrad Khamesee, M.; Roa, W.; Amirfazli, A. Magnetic Targeting of Aerosol Particles for Cancer Therapy. *J. Magn. Magn. Mater.* **2005**, *293* (1), 442−449.
(23) Niazi, S. B.; Littlejohn, D.; Halls, D. J. Rapid Partial Digestion of Biological Tissues with Nitric Acid for the Determination of Trace Elements by Atomic Spectrometry. *Analyst* **1993**, *118* (7), 821−825.
(24) Faul, F.; Erdfelder, E.; Buchner, A.; Lang, A.-G. Statistical Power Analyses Using G * Power 3. 1 : Tests for Correlation and Regression Analyses. *Behav. Res. Methods* **2009**, *41* (4), 1149−1160.
(25) Faul, F.; Erdfelder, E.; Lang, A.-G.; Buchner, A. G*Power 3: A Flexible Statistical Power Analysis Program for the Social, Behavioral, and Biomedical Sciences. *Behav. Res. Methods* **2007**, *39* (2), 175−191.
(26) Sham, J. O. H.; Zhang, Y.; Finlay, W. H.; Roa, W. H.; Löbenberg, R. Formulation and Characterization of Spray-Dried Powders Containing Nanoparticles for Aerosol Delivery to the Lung. *Int. J. Pharm.* **2004**, *269* (2), 457−467.
(27) Haslam, G.; Richter, M.; Wyatt, D.; Ye, Q. Z.; Kitos, P. Estimating the Number of Viable Animal Cells in Multiwell Culture - A Tetrazolium-Based Assay. *Anal. Biochem.* **2005**, *336* (2), 187−195.
(28) Lewinski, N.; Colvin, V.; Drezek, R. Cytotoxicity of Nanoparticles. *Small* **2008**, *4* (1), 26−49.
(29) Taylor, R. M.; Monson, T. C.; Gullapalli, R. R. Influence of Carbon Chain Length on the Synthesis and Yield of Fatty Amine-Coated Iron-Platinum Nanoparticles. *Nanoscale Res. Lett.* **2014**, *9*, 306.
(30) Chertok, B.; Cole, A.; David, A.; Yang, V. Comparison of Electron Spin Resonance Spectroscopy and Inductively-Coupled Plasma Optical Emission Spectroscopy for Biodistribution Analysis of Iron-Oxide Nanoparticles. *Mol. Pharmaceutics* **2010**, *7* (2), 375−385.
(31) Cole, A. J.; David, A. E.; Wang, J.; Galbán, C. J.; Yang, V. C. Magnetic Brain Tumor Targeting and Biodistribution of Long-Circulating PEG-Modified, Cross-Linked Starch-Coated Iron Oxide Nanoparticles. *Biomaterials* **2011**, *32* (26), 6291−6301.
(32) Su, W. C.; Cheng, Y. S. Deposition of Man-Made Fibers in Human Respiratory Airway Casts. *J. Aerosol Sci.* **2009**, *40* (3), 270−284.
(33) Xie, Y.; Longest, P. W.; Xu, Y. H.; Wang, J. P.; Wiedmann, T. S. Vitro and in Vivo Lung Deposition of Coated Magnetic Aerosol Particles. *J. Pharm. Sci.* **2010**, *99* (11), 4658−4668.
(34) Tewes, F.; Ehrhardt, C.; Healy, A. M. Superparamagnetic Iron Oxide Nanoparticles (SPIONs)-Loaded Trojan Microparticles for Targeted Aerosol Delivery to the Lung. *Eur. J. Pharm. Biopharm.* **2014**, *86* (1), 98−104.
(35) McBride, A. A.; Muttil, P. A Pilot Study Targeting Nano-in-Microparticles (NIMs) in Rat Lungs Ex Vivo. *Respir. Drug Delivery* **2013**, *2* (May), 42.
(36) McBride, A. A.; Lamoureux, L. R.; Price, D. N.; Muttil, P. Novel Preparation and Characterization of Magnetic Nano-in-Microparticle Dry Powders for Directed Drug Delivery : An Application to Lung Cancer. *Respir. Drug Delivery* **2012**, *4*, 1−6.
(37) Huang, G.; Chen, H.; Dong, Y.; Luo, X.; Yu, H.; Moore, Z.; Bey, E. A.; Boothman, D. A.; Gao, J. Superparamagnetic Iron Oxide Nanoparticles: Amplifying ROS Stress to Improve Anticancer Drug Efficacy. *Theranostics* **2013**, *3* (2), 116−126.
(38) Healy, A. M.; Amaro, M. I.; Paluch, K. J.; Tajber, L. Dry Powders for Oral Inhalation Free of Lactose Carrier Particles. *Adv. Drug Delivery Rev.* **2014**, *75*, 32−52.
(39) Stahlhofen, W.; Moller, W. Behaviour of Magnetic Micro-Particles in the Human Lung. *Radiat. Environ. Biophys.* **1993**, *32* (3), 221−238.
(40) Polyak, B.; Friedman, G. Magnetic Targeting for Site-Specific Drug Delivery: Applications and Clinical Potential. *Expert Opin. Drug Delivery* **2009**, *6* (1), 53−70.
(41) Prijic, S.; Prosen, L.; Cemazar, M.; Scancar, J.; Romih, R.; Lavrencak, J.; Bregar, V. B.; Coer, A.; Krzan, M.; Znidarsic, A.; Sersa, G. Surface Modified Magnetic Nanoparticles for Immuno-Gene Therapy of Murine Mammary Adenocarcinoma. *Biomaterials* **2012**, *33* (17), 4379−4391.
(42) Tonnis, W.; Bagerman, M.; Weij, M.; Sjollema, J.; Frijlink, H.; Hinrichs, W.; de Boer, A. A Novel Aerosol Generator for Homogenous Distribution of Powder over the Lungs after Pulmonary Administration to Small Laboratory Animals. *Eur. J. Pharm. Biopharm.* **2014**, *88* (3), 1056−1063.
(43) Hoppentocht, M.; Hoste, C.; Hagedoorn, P.; Frijlink, H. W.; de Boer, A. H. Vitro Evaluation of the DP-4M PennCentury insufflator. *Eur. J. Pharm. Biopharm.* **2014**, *88* (1), 153−159.
(44) Duret, C.; Merlos, R.; Wauthoz, N.; Sebti, T.; Vanderbist, F.; Amighi, K. Pharmacokinetic Evaluation in Mice of Amorphous Itraconazole-Based Dry Powder Formulations for Inhalation with High Bioavailability and Extended Lung Retention. *Eur. J. Pharm. Biopharm.* **2014**, *86* (1), 46−54.
(45) Takeda, S.; Mishima, F.; Fujimoto, S.; Izumi, Y.; Nishijima, S. Development of Magnetically Targeted Drug Delivery System Using Superconducting Magnet. *J. Magn. Magn. Mater.* **2007**, *311* (1), 367−371.
(46) Price, D. N.; McBride, A. A.; Anton, M.; Kusewitt, D. F.; Norenberg, J. P.; MacKenzie, D. A.; Thompson, T. A.; Muttil, P. Longitudinal Assessment of Lung Cancer Progression in Mice Using the Sodium Iodide Symporter Reporter Gene and SPECT/CT Imaging. *PLoS One* **2016**, *11* (12), e0169107.

DOI: 10.1021/acs.molpharmaceut.7b00532
Mol. Pharmaceutics 2017, 14, 4741−4750